SIMULATIONS OF ENERGETIC PARTICLE DRIVEN INSTABILITIES AND FAST PARTICLE REDISTRIBUTION IN EAST TOKAMAK

WEI SHEN
Institute of Plasma Physics, Chinese Academy of Sciences
Hefei, China
Email: shenwei@ipp.ac.cn

YOUBIN PEI
Institute of Plasma Physics, Chinese Academy of Sciences
University of Science and Technology of China
Hefei, China

YINGFENG XU
Institute of Plasma Physics, Chinese Academy of Sciences
Hefei, China

AUTHOR et al.

Abstract

Instabilities driven by energetic particles including fishbones and Alfvén eigenmodes, together with fast particle loss and redistribution due to resonant magnetic perturbations (RMPs), have been investigated numerically with codes M3D-K, MEGA, and GYCAVA in EAST tokamak. Firstly, hybrid simulations with the global kinetic-magnetohydrodynamic code M3D-K have been carried out to investigate the beam-driven fishbone in EAST experiment. The results are consistent with the experimental measurement with respect to mode frequency and mode structure. Nonlinear simulations show that the frequency of the fishbone chirps up and down with corresponding hole-clump structures in phase space, consistent with the Berk-Breizman theory. A high frequency beta-induced Alfvén eigenmode is excited during the nonlinear evolution. Secondly, two kinetic-MHD codes, namely MEGA and M3D-K, have been applied to study fast ion driven toroidal Alfvén eigenmodes (TAEs) in EAST tokamak. Parameter scans show that the frequency and growth rate of TAEs simulated by the two codes agree with each other. The analysis of the resonant interaction between the TAE and fast ions shows that the TAE exchanges energy with the co-current passing particles with parallel velocity equaling to 1/3 or 1/5 of the Alfvén speed on the magnetic axis. Thirdly, the effects of RMPs on the loss and heat load of fast ions are investigated numerically by the orbit following code GYCAVA for EAST tokamak. The loss fraction increases when the RMP coil current increases. Without RMPs, the initial positions of lost fast ions are near the edge on the high field side. However, the initial positions of lost fast ions are located near the edge on both the low and high field side with RMPs, and the fraction of lost fast ions initially deposited near the low field side increases when the RMP coil current becomes larger. These results would provide guidance for future EAST experiments.

1. INTRODUCTION

Energetic physics is a crucial issue in burning plasmas of magnetic fusion reactors such as the international thermonuclear experimental reactor (ITER) [1]. Energetic particle driven instabilities, such as fishbones and various Alfvén eigenmodes, can induce energetic particle loss, degrade fast particle confinement, and even lead to serious damage of the first wall. The fishbone, which was first discovered in the poloidal divertor experiments (PDX) [2], is typically an n=1 internal mode with dominant poloidal mode number m=1. In tokamaks, the shear Alfvén continuous spectrum can be broken up by toroidicity, and Toroidal Alfvén eigenmodes are discrete shear Alfvén eigenmodes which can exist inside the toroidicity-induced continuum gaps [3,4]. The resonant magnetic perturbations induced by external coils can break the axisymmetry in tokamaks. As a result, resonant magnetic perturbations can lead to redistribution and even significant loss of energetic particles. In the paper, Instabilities driven by energetic particles including fishbones and Toroidal Alfvén eigenmodes, together with fast particle loss and redistribution due to resonant magnetic perturbations, have been investigated numerically with codes M3D-K [5], MEGA [6], and GYCAVA [7] in EAST tokamak.

2. SIMULATION OF FISHBONE INSTABILITY

In 2014, the fishbone instability was observed in EAST experiment with neutral beam injection (NBI) heating for the first time [8]. In this section, hybrid simulations with the global kinetic-magnetohydrodynamic (MHD) code M3D-K have been carried out to investigate the beam-driven fishbone in EAST experiment [9]. Equilibrium profiles and parameters are chosen base on the Shot #48605 of the EAST experiment. The injection

energy of NBI is 60 keV. As beam particles with energies of 30 keV and 20 keV are also injected, a multiple energy component slowing-down distribution is used for the fast ions, which has been fitting with the beam ion distribution obtained from NUBEAM code [10].

Linear simulation results are present firstly. The scanning of mode frequency and linear growth rate as a function of fast ion pressure fraction $P_{hot,0}/P_{total,0}$ with fixed total pressure has been performed. As show in figure 1, the ideal internal kink mode is unstable at zero beam ion pressure, $P_{hot,0}/P_{total,0} = 0$. When $P_{hot,0}/P_{total,0}$ increases from 0 to 0.15, the mode is stabilized due to the kinetic effects of beam ions. However, when $P_{hot,0}/P_{total,0} > 0.2$, the fishbone instability is excited. When $P_{hot,0}/P_{total,0}$ increases further, the fishbone with mode frequency around 0.03 ω_A transits to a beta-induced Alfvén eigenmode (BAE) with higher mode frequency $\omega \sim 0.13\ \omega_A$ and mode number m=n=1, where $\omega_A = V_{A0}/R_0$, V_{A0} is the Alfvén speed calculated at the magnetic axis, and R_0 is the major radius. Moreover, there exits a transient range of $P_{hot,0}/P_{total,0}$ where both the two modes can co-exist in the linear phase, corresponding to the transition phase from the fishbone to BAE. According to EAST experimental measurements, The pressure fraction $P_{hot,0}/P_{total,0}$ is around 0.25, the corresponding mode frequency from the M3D-K simulation is $f_{sim} = (0.022\ \omega_A)/(2\pi) = 6.99$ kHz, which is consistent with the experiment measured mode frequency $f_{exp} = 5\sim7$ kHz [8]. In addition, the simulated fishbone mode structure agrees well with the experimental measurements, as shown in figure 2. The scanning of the fishbone instability as a function of injection energy and pitch angle shows that the fishbone is mainly driven by trapped fast ions with energy less than 30 keV.

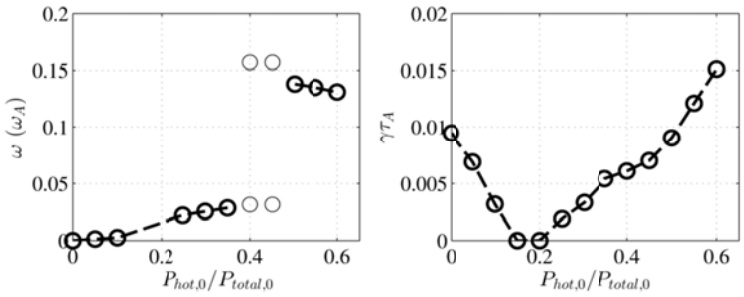

FIG. 1. Mode frequency and linear growth rate as a function of fast ion pressure fraction.

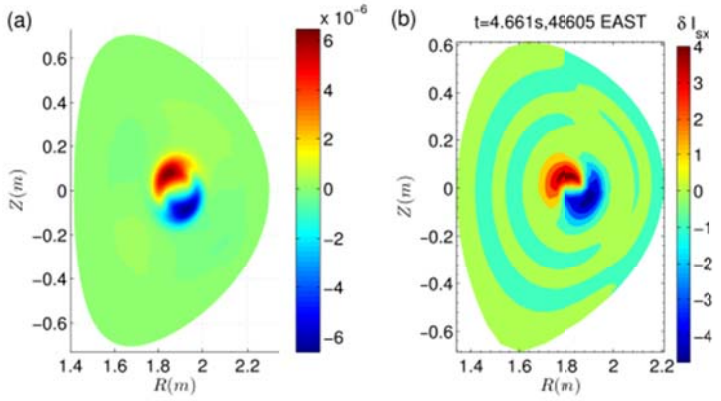

FIG. 2. Mode structure of fishbone instability. (a) M3D-K simulation result; (b) EAST experimental measurement.

The nonlinear dynamics of the low fishbone is analyzed with $P_{hot,0}/P_{total,0} = 0.3$. The time evolution of the mode amplitude shows that the fishbone instability first grows and then saturates from $t \approx 1500\ \tau_A$, where $\tau_A = R_0/V_{A0}$ is the Alfvén time. Correspondingly, the mode frequency starts to chirp up and down at $t \approx 1200\ \tau_A$ with dominant downward branch. Moreover, a high frequency BAE with mode frequency around $0.166\ \omega_A$ emerges at $t \approx 3000\ \tau_A$ and persists until $t \approx 5000\ \tau_A$. The change of the beam ion distribution df is consistent with the mode frequency evolution. In the linear phase, the large df structure corresponds to the resonant condition of the linear mode frequency. In the early nonlinear phase, hole and clump structures emerge, and the clump corresponds to the resonant condition of down-chirping mode frequency, while the hole

corresponds to the up-chirping mode frequency. In later nonlinear phase after the emergence of the high frequency BAE, one more resonant condition is found to agree with the BAE frequency. Finally the large d*f* structure becomes broader, which indicates that the flattening region of the distribution function expands inward and outward in radial direction at the central region of the plasma. The results of hole-clump structure and frequency chirping are consistent with the Berk-Breizman theory, which has been used to explain the TAE up-down chirping near marginal instability [11,12].

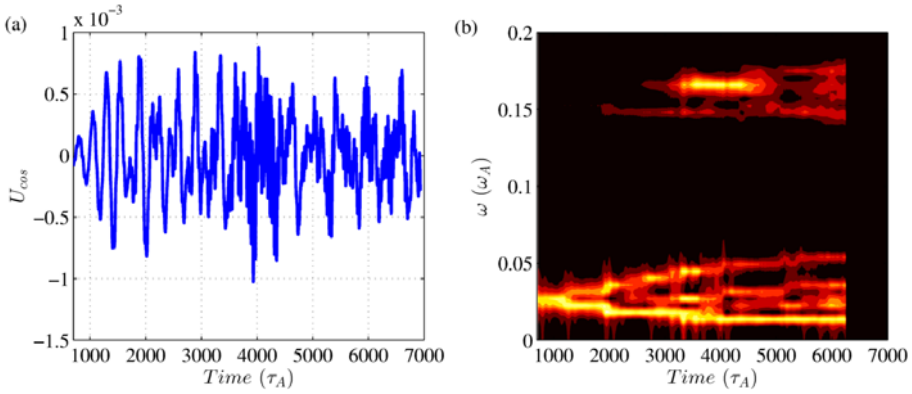

FIG. 3. Time evolution of the mode amplitude and frequency of the fishbone instability.

The measured fishbone frequency in the EAST experiment chirps down, which is consistent with the simulation results. However, the high frequency BAE was not observed in the experiment. The possible reason is that the frequency resolution in the experiment measurement is limited. The maximum of the measured frequency from the diagnosis is around 50 kHz as the sampling rate is 100 k. In addition, the frequency of the thermal plasma rotation is around 13 kHz. As a result, the maximum mode frequency from experimental measurement is around 37 kHz, which is smaller than the BAE frequency $0.166\ \omega_A$ corresponding to 52.5 kHz.

Furthermore, for the transient case of beam pressure fraction $P_{hot,0}/P_{total,0}$ = 0.4 where the fishbone and BAE are simultaneously excited in the linear phase, only one mode appears to be dominant in the nonlinear phase with frequency jumps up and down during evolution. The frequency jumping phenomena have been observed in other tokamak experiments. In future, EAST experiment will be planned to verify the prediction of high-frequency BAE and frequency jumping.

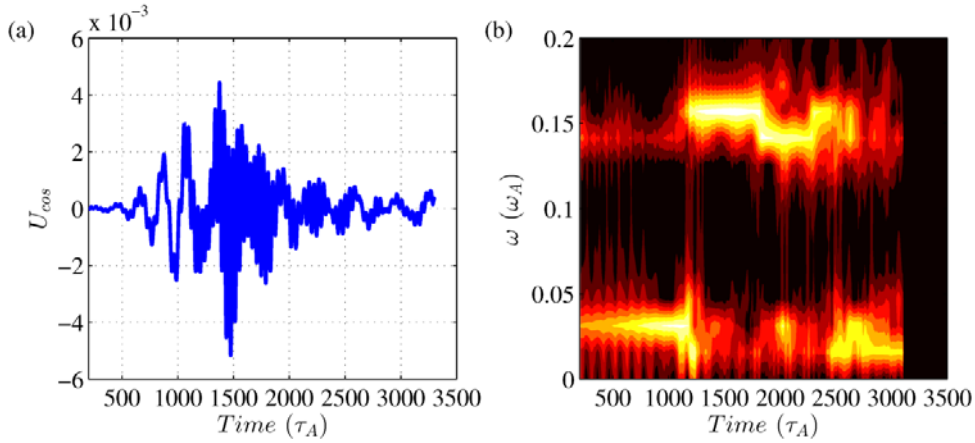

FIG. 4. Time evolution of the mode amplitude and frequency of the mode with $P_{hot,0}/P_{total,0}$ = 0.4.

3. SIMULATION OF TOROIDAL ALFVÉN EIGENMODES

In this section, two kinetic-MHD codes, namely MEGA and M3D-K, have been applied to study toroidal Alfvén eigenmodes (TAEs) driven by fast ions in EAST tokamak [13]. The parameters and initial profiles are based on

the EAST discharge #38300 at 3900 ms. The equilibrium used by MEGA code is reconstructed directly from EFIT code [14], and the equilibrium used in M3D-K code is generated from VMEC code [15] with up-down symmetric which is reconstructed based on the EFIT equilibrium. The beam ions in both codes are described using the anisotropic slowing down distribution with injection energy 80 keV.

In the simulation, the dominant toroidal harmonic of the simulated mode is *n*=-1, which indicates that the toroidal propagation direction of the mode is the co-current direction. As a result, it is consistent with the general rules for the propagation direction of Alfvén eigenmodes driven by fast ions in tokamak plasmas [16]. As shown in figure 5, the radial profiles of perturbed poloidal magnetic field with different poloidal harmonics and toroidal harmonic *n*=-1 indicates that the *m*=1 and *m*=2 poloidal harmonics are dominant compared with other *m* components, and the radial location of the dominant harmonics is localized at $\psi = 0.4$ with frequency around 96 kHz， where $\psi = \sqrt{\bar{\psi}_p}$ and $\bar{\psi}_p$ is the normalized poloidal magnetic flux. The *n*=-1 Alfvén continua has been calculated by the MHD eigenvalue code GTAW [17], and it is shown that the mode is inside the gap which is formed due to the coupling between *m*=1 and *m*=2 harmonics. As a result, the mode destabilized by the beam ions in the simulation is identified as a TAE.

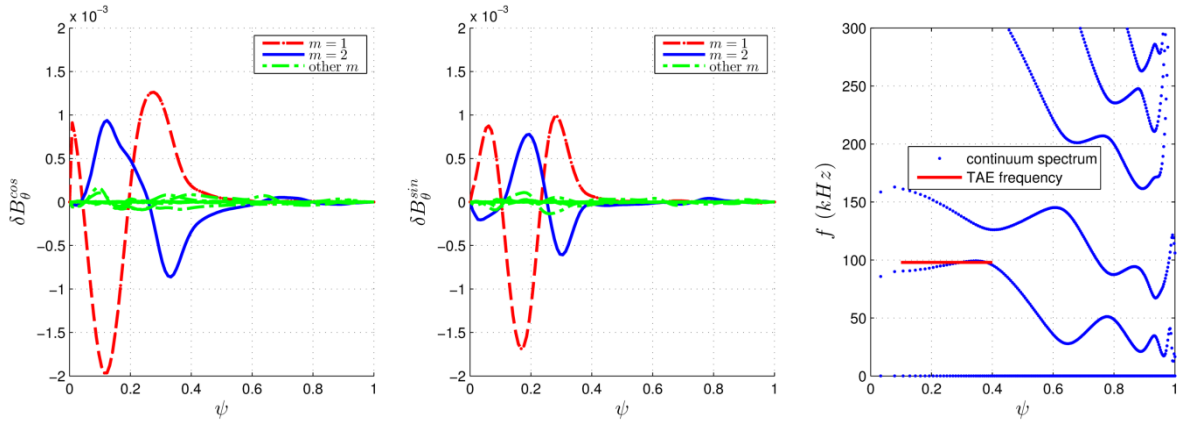

FIG. 5. Radial profiles of polodal harmonics of the perturbed poloidal magnetic field, and the Alfvén continua with n=-1.

As shown in figure 6, the mode structures of toroidal electric field in the poloidal plane simulated by MEGA and M3D-K show good agreement between the two codes, and *m*=1 and *m*=2 poloidal harmonics are found to be dominant with *m*=1 component larger than *m*=2 component, which is consistent with the results of perturbed poloidal magnetic field in radial direction. In addition, parameter scans show good agreement between the two codes with respect to the dependence of the TAE growth rate and the real frequency on the fast ions on-axis beta, injection beam energy and central pitch angle parameter. As the mode frequency is almost fixed around 96 kHz, figure 7 shows the linear growth rate as a function of the fast ions on-axis beta, injection beam energy and central pitch angle parameter, respectively.

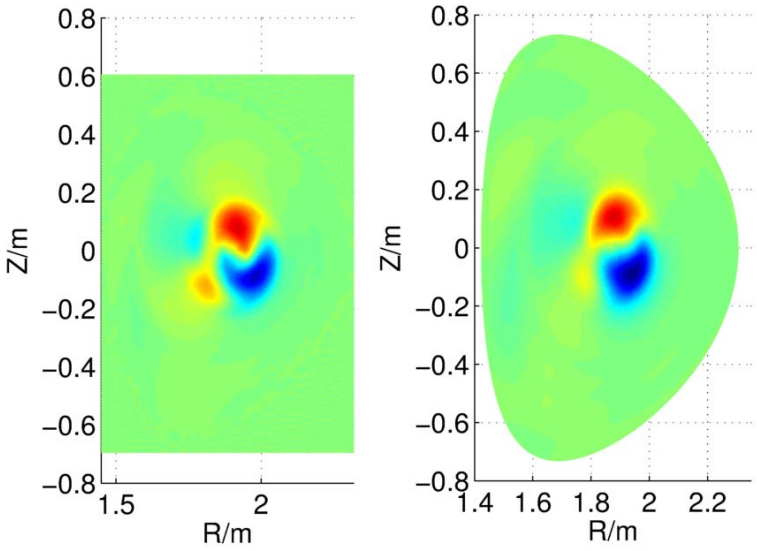

FIG. 6. Mode structure of the TAE. Left: MEGA simulation result; Right: M3D-K simulation result.

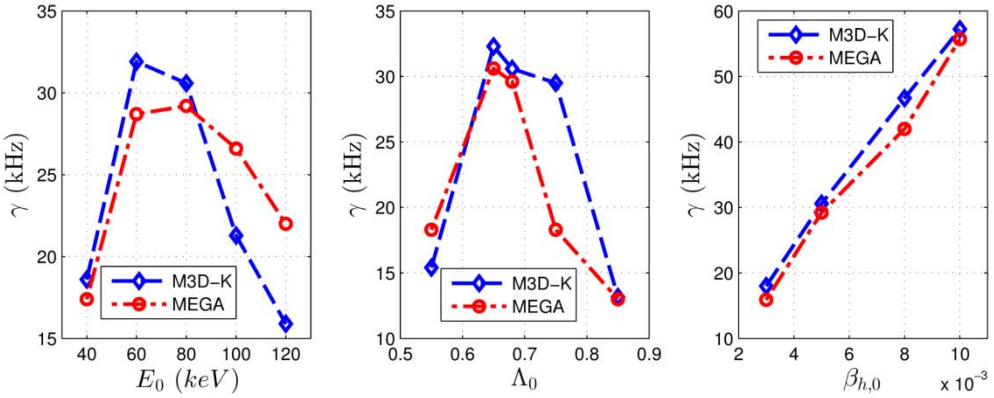

FIG. 7. The TAE growth rate as a function of beam injection energy, pitch angle parameter, and beam ion central beta.

In order to understand the mechanism of the TAE driven by fast ions better, 1000 fast particles with a large value of $|df|$ are picked out to check whether they are resonant with the TAE. As the wave-particle resonant condition is given by [18] $l = (\omega - n\omega_\phi)/\omega_\theta$, where ω is the mode frequency, *n* is the toroidal mode number, *l* is the resonant number and should be an integer if the resonant condition is satisfied, ω_ϕ is the toroidal transit frequency of the particle, and ω_θ is the poloidal transit frequency. For the 1000 chosen particles, it is found that *l* is close to zero for most particles, which indicates that these particles are resonant with the TAE. As most of the particles are passing particles, the poloidal and toroidal transit frequencies of the particles are approximated as $\omega_\theta = v_\parallel/(qR)$, and $\omega_\phi = v_\parallel/R$, where $v_\parallel$ is the particle parallel velocity, q is the safety factor, and *R* is the major radius. Moreover, the TAE frequency is $\omega = V_{A0}/(2qR)$ with $q = |(2m+1)/(2n)|$. As a result, the parallel velocity is obtained as $v_\parallel = V_{A0}/(2l - 2m - 1)$. In the simulation, $l = 0$ and the dominant mode numbers are *m*=1, 2, so the particles with $v_\parallel = -V_{A0}/3$ or $v_\parallel = -V_{A0}/5$ are resonant with the TAE.

In the above, the TAE driven by co-current passing particles has been analyzed. Moreover, the TAE destabilized by the counter-current passing ions is also investigated. It is found that the same TAE is driven unstable but it has much smaller growth rate compared with the co-current fast ions driven TAE. One possible reason to explain this is that the overlapping region between the counter-current passing fast ion orbits and the TAE is smaller than the co-current passing fast ions. Thus, the wave-particle energy exchange for the counter-current passing beam ions is weaker.

4. RESONANT MAGNETIC PERTURBATIONS INDUCED FAST ION TRANSPORT

In this section, the effects of RMPs on the loss, heat load, and redistribution of fast ions are investigated numerically by the orbit following code GYCAVA for EAST tokamak. The parameters and initial profiles are based on the EAST discharge #55272, and fast ions are generated by co-tangent NBI with R_{tan}=1.264 m and birth energy E_0=50 keV. In addition, RMPs with toroidal mode number n=1 are calculated by MARS-F code [19] without plasma response.

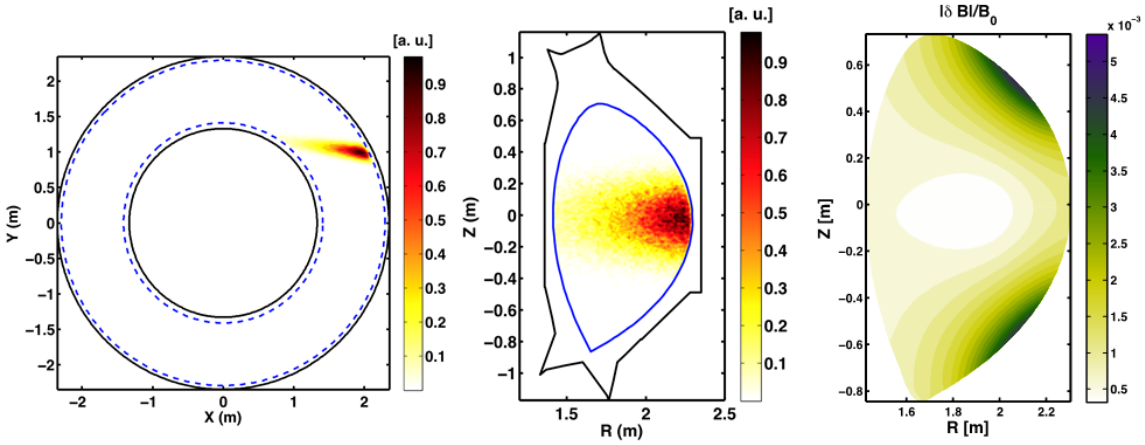

FIG. 8. NBI deposition (left:top view;middle:poloidal cross-section) and RMPs (right) on EAST.

The loss of fast ions increases when the RMP coil current increases. When the RMP coil current is sufficient large, the fast ion loss due to magnetic islands generated by the RMPs can be much larger than the loss induced by magnetic drift. As shown in figure 9, the loss fraction of fast ions is around 2% without RMPs. When the RMP coil current I_{RMP}=10 kAt, the loss fraction becomes much larger and increases to around 8%. The loss fraction increases further larger to around 16% when I_{RMP}=15 kAt. The loss fraction of power is similar to the loss fraction of fast ions. In addition, The fast ion loss with different boundary conditions are compared, and it is found that the loss fraction of fast ions with wall boundary is less than the loss fraction with the last closed flux surface (LCFS), and the difference between these two loss fractions becomes smaller when I_{RMP} increases.

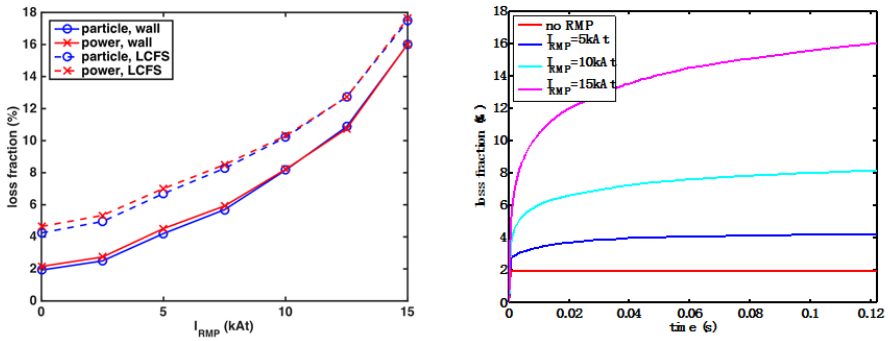

FIG. 9. Loss fraction of fast ions as a function of the RMP coil current and time, respectively.

Figure 10 shows the initial and final positions of lost fast ions with different RMP coil currents. Without RMPs, the initial positions of lost fast ions are near the edge on the high field side. However, the initial positions of lost fast ions are located near the edge on both the low and high field side with RMPs, and the fraction of lost fast ions initially deposited near the low field side increases when I_{RMP} becomes larger. The mechanism why RMPs induce fast ion loss is that RMPs break axisymmetry and generate drift islands of fast ions, and stochasticity due to drift island overlapping will cause fast ions to run across the drift islands and induce fast ion loss [7]. The fast ions are finally lost at the outer wall above the mid-plane and near the divertors.

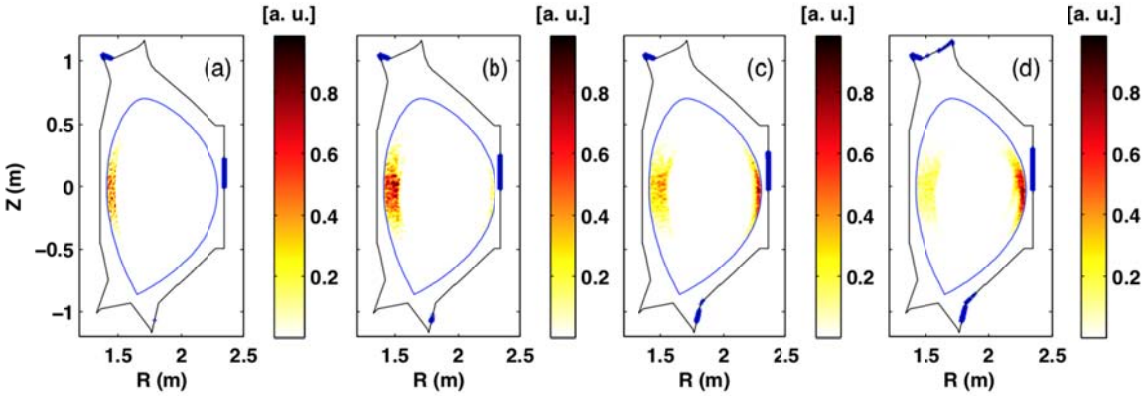

FIG. 10. Initial and final positions of lost fast ions. (a) without RMPs; (b) I_{RMP}=5 kAt; (c) I_{RMP}=10 kAt; (d) I_{RMP}=15 kAt.

Figure 11 shows the heat loads distributed in the poloidal and toroidal angels for four different cases, it is found that the poloidal distributions of the heat loads are very local and manly located near the upper divertor and on the outer wall above the mid-plane. Without RMPs, the toroidal distributions of the heat loads are relatively uniform. With RMPs, the heat load is mainly on the outer wall above the mid-plane with maximum value around toroidal angel equaling 200°, which is related to the counter-clockwise direction of B_t for the co-current NBI.

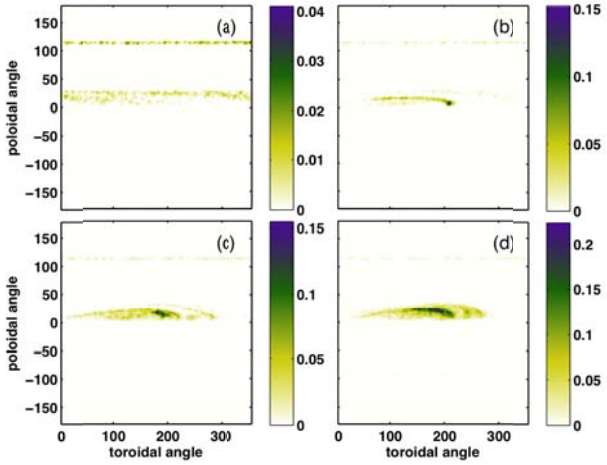

FIG. 11. Heat load for differnt RMP coil currents. (a) without RMPs; (b) I_{RMP}=5 kAt; (c) I_{RMP}=10 kAt; (d) I_{RMP}=15 kAt.

5. SUMMARY AND CONCLUSIONS

In conclusion, instabilities driven by energetic particles including fishbones and Alfvén eigenmodes, together with fast particle loss and redistribution due to RMPs, have been investigated numerically with codes M3D-K, MEGA, and GYCAVA in EAST tokamak. Firstly, hybrid simulations with the global kinetic- MHD code M3D-K have been carried out to investigate the beam-driven fishbone in EAST experiment. Linear simulation result shows a low frequency fishbone instability driven by trapped beam ions via precessional resonance. The simulated fishbone frequency and mode structure agree well with experimental measurements. Nonlinear simulations show that the frequency of the fishbone chirps up and down with corresponding hole-clump structure formation and movement in the phase space. The nonlinear evolution of frequency chirping and hole-clump movement agrees with Berk–Breizman hole-clump theory. Furthermore, a high frequency BAE is excited during the nonlinear evolution. Secondly, two kinetic-MHD codes MEGA and M3D-K, have been applied to study fast ion driven TAEs in EAST tokamak. Parameter scans show good agreement between the two codes with respect to the dependence of the TAE growth rate and the real frequency on the fast ions on-axis beta,

injection beam energy and central pitch angle parameter. The analysis of the resonant interaction between the TAE and fast ions shows that the TAE exchanges energy with the co-current passing particles with parallel velocity equaling to 1/3 or 1/5 of the Alfvén speed on the magnetic axis. In addition, the TAE destabilized by the counter-current passing ions is also analyzed and found to have much smaller growth rate than that of the co-current fast ions driven TAE. Thirdly, the effects of RMPs on the loss and heat load of fast ions are investigated numerically by the orbit following code GYCAVA for EAST tokamak. The loss fraction increases when the RMP coil current increases. Without RMPs, the initial positions of lost fast ions are near the edge on the high field side. However, the initial positions of lost fast ions are located near the edge on both the low and high field side with RMPs, and the fraction of lost fast ions initially deposited near the low field side increases when the RMP coil current becomes larger. The heat loads distributed in the poloidal and toroidal angels are investigated, and it is found that the poloidal distributions of the heat loads are very local and manly located near the upper divertor and on the outer wall above the mid-plane. Without RMPs, the toroidal distributions of the heat loads are relatively uniform. With RMPs, the heat load is mainly on the outer wall above the mid-plane with maximum value around toroidal angel equaling 200°. These results would provide guidance for future EAST experiments.

ACKNOWLEDGEMENTS

Numerical computations were performed on the ShenMa High Performance Computing Cluster at the Institute of Plasma Physics, Chinese Academy of Sciences. This work is supported by the National Key R&D Program of China under Grant No. 2017YFE0300400, and the National Natural Science Foundation of China under Grant Nos. 11775265, 11405174, 11475219, 11775268, 11505240, 11375196, 11575246, 11475220, 11575251, 11575249, 11605245 and 11505022, and the CASHIPS Director's Fund under Grant No. YZJJ201510, and the Department of Energy Scientific Discovery through Advanced Computing (SciDAC) under Grant No. DE-AC02-09CH11466, and the National ITER program of China under Contract No. 2014GB113000, and the JSPS-NRF-NSFC A3 Foresight Program in the field of Plasma Physics (NSFC No. 11261140328), and the National Magnetic Confinement Fusion Energy Research Program under Grant No. 2015GB110005.

REFERENCES

[1] FASOLI A. et al., Nuclear Fusion, Nucl. Fusion **47** 2007 S264
[2] MCGUIRE K. et al., Physics Review Letters, Phys. Rev. Lett. **50** 1983 891-5
[3] CHENG C. Z., CHANCE M. S., Physics of Fluids, Phys. Fluids **29** 1986 3695
[4] CHENG C. Z., CHEN L., CHANCE M. S., Annals of Physics, Ann. Phys. **161** 1984 21
[5] FU G. Y., Physics of Plasmas, Phys. Plasmas **13** 2006 052517.
[6] TODO Y. et al., Physics of Plasmas, Phys. Plasmas **2** 1995 2711.
[7] XU Y. F. et al., Physics of Plasmas, Phys. Plasmas **25** 2018 012502.
[8] XU L. Q. et al., Physics of Plasmas, Phys. Plasmas **22** 2016 122510.
[9] SHEN W. et al., Nuclear Fusion, Nucl. Fusion **57** 2017 116035.
[10] PANKIN A. et al., Computer Physics Communications, Comput. Phys. Commun. **159** 2004 157-84.
[11] BERK H. L. et al., Physics Letters A, Phys. Lett. A **234** 1997 213.
[12] BERK H. L. et al., Physics of Plasmas, Phys. Plasmas **6** 1999 3102.
[13] PEI Y. B. et al., Physics of Plasmas, Phys. Plasmas **25** 2018 052503.
[14] LAO L. et al., Nuclear Fusion, Nucl. Fusion **25** 1985 1421.
[15] HIRSHMAN S. et al., Computer Physics Communications, Comput. Phys. Commun. **43** 1986 143.
[16] TODO Y. et al., AIP Conference Proceedings, AIP Conf. Proc. **1478** 2012 141.
[17] HU Y. et al., Physics of Plasmas, Phys. Plasmas **21** 2014 052510.
[18] TODO Y., SATO T., Physics of Plasmas, Phys. Plasmas **21** 2014 052510.
[19] LIU Y. Q. et al., Physics of Plasmas, Phys. Plasmas **7** 2000 3681.